International Journal of Biological Macromolecules 330 (2025) 147940

Contents lists available at ScienceDirect

International Journal of Biological Macromolecules

journal homepage: www.elsevier.com/locate/ijbiomac

The promotion of cartilage regeneration by injectable photocurable gelatin hydrogel loaded with auto-concentrated growth factor

Xiaoyan Zeng [a,1], Lixiang Zhang [b,c,1], Zewen Wang [b,1], Piming Nie [b], Zhengchao Yuan [d], Xiumei Mo [d], Chenhui Cai [b,*], Chao Zhang [b,*], Yuan Xu [b,*]

[a] Department of General Surgery, Xinqiao Hospital, Army Military Medical University, No. 183, Xinqiao Street, Shapingba District, Chongqing, 400037, PR China
[b] Department of Orthopaedics, Xinqiao Hospital, Army Military Medical University, No. 183, Xinqiao Street, Shapingba District, Chongqing, 400037, PR China
[c] Department of health management, Characteristic Medical Center of Chinese People's Armed Police Force, 220 Chenglin Road, Hedong District, Tianjin, China
[d] State Key Laboratory for Modification of Chemical Fibers and Polymer Materials, Shanghai Engineering Research Center of Nano-Biomaterials and Regenerative Medicine, College of Biological Science and Medical Engineering, Donghua University, 201620, Shanghai, PR China

ARTICLE INFO

Keywords:
Cartilage regeneration
Concentrated growth factor
Hydrogel

ABSTRACT

The self-healing capability of injured cartilage is very limited. Concentrated growth factor (CGF) can promote tissue repair, cell regeneration and wound healing, It is widely used in the fields of cosmetology, wound repair and dental implantation. CGF is extracted from autologous blood by centrifugation, which is enriched with different types of growth factors as well as fibrin. Here, we have developed CGF-loaded gelatin methacryloyl (GM) hydrogels for cartilage tissue repair. GM@CGF hydrogel can promote cell migration, and they can additionally increase cell proliferation as well as the migration of chondrocytes *in vitro*. These *in situ* injectable GM@CGF hydrogels were transplanted into a rabbit distal femur cartilage defect model; the defect was repaired and was filled with transparent and fibrous cartilage with a smooth surface. The repaired cartilage tissues showed high expression of COL II and SOX9. In conclusion, GM@CGF hydrogels exhibit a satisfactory cartilage repair capability in rabbit, which may have broad application prospects.

1. Introduction

Cartilage, a critical component of human skeletal system, covers articular surfaces, providing a smooth and lubricated interface that reduces friction in synovial joints and facilitates load transmission [1–3]. Unlike bone tissue, cartilage lacks blood vessels, nerves, or lymphatic vessels, leading to poor nutrient supply and limited cell infiltration. Consequently, cartilage injuries caused by trauma, inflammation, or sustained mechanical stress require functional scaffolds to promote regeneration [4–6]. Cartilage repair is further limited by different types of factors, including insufficient intrinsic regeneration ability of cartilage, ischemic/hypoxic microenvironment at injury site, and lack of suitable biomaterials and transplantation methods [5,7–10].

Growth factors can play a pivotal role in cartilage tissue repair as they can promote the proliferation, differentiation, and extracellular matrix (ECM) synthesis of chondrocytes. Common regulatory growth factors include matrix metalloproteinase (MMP), transforming growth factor-beta (TGF-β), and fibroblast growth factor (FGF) [11–13]. These bioactive cues can accelerate cartilage tissue repair by stimulating the proliferation of chondrocytes as well as enhancing ECM synthesis [11,14]. Indeed, different types of approaches have been leveraged for the delivery of growth factors, such as topical injection, carrier implantation, and biomaterial-based systems [15,16].

Over the past decades, tissue engineering-integrating biomaterials, cells, and bioactive factors-has provided novel therapeutic strategies for tissue repair [5,17–19]. Concentrated growth factors (CGFs), the third-generation plasma extract, are second to platelet-rich fibrin (PRF) and platelet-rich plasma (PRP). The CGFs are acquired by continuous variable-speed centrifugation; the latter activates and disrupts platelets to release potent growth factor clusters [20]. CGFs contain abundant fibrin, leukocytes, $CD34^+$ cells, and growth factors (*e.g.*, fibroblast growth factor (FGF), epithelial growth factor (EGF), vascular endothelial growth factor (VEGF), insulin-like growth factor (IGF), platelet-derived growth factor (PDGF), transforming growth factor-beta (TGF-β), *etc.*). The concentration of growth factors is 7–22 times higher in CGF than that of the whole blood. As a bioactive material, CGF can promote

* Corresponding author.
E-mail addresses: chenhuicai1113@tmmu.edu.cn (C. Cai), tmmuzc@tmmu.edu.com (C. Zhang), xuyuan88@tmmu.edu.com (Y. Xu).
[1] Xiaoyan Zeng, Lixiang Zhang and Zewen Wang are co-first authors.

https://doi.org/10.1016/j.ijbiomac.2025.147940
Received 28 February 2025; Received in revised form 18 September 2025; Accepted 25 September 2025
Available online 29 September 2025

cell proliferation, cell differentiation, and cell migration. Moreover, CGF can enhance angiogenesis as well as facilitate tissue repair [20–22]. Clinical studies in jaw cyst surgery and rheumatoid arthritis treatment have shown that CGFs can accelerate healing, reduce recovery time, and improve bone healing quality, which may have implications for bone defect repair, implant fixation, and grafting [23–25].

However, there are some limitations for the application of CGFs for cartilage tissue repair: (1) insufficient mechanical strength to support joint dynamic loading; (2) rapid *in vivo* degradation, leading to fast release of growth factors as well as their unstable concentrations; and (3) poor plasticity and adhesion, which may impede long-term retention in irregular defects, and compromise regeneration and tissue integrity. In contrast, GM hydrogels offer distinct advantages: photo-crosslinking ability of hydrogels may enable minimally invasive *in situ* rapid molding to fill complex defect morphologies; (b) 3D porous network structure of hydrogels may provide mechanical buffering akin to natural cartilage; (c) these hydrogels may enable sustained and controlled release of growth factors/drugs; and (d) create a biomimetic microenvironment to promote the migration, proliferation, and ECM secretion of chondrocyte.

In the preliminary test, CGFs were loaded into GM hydrogel through physical blending, which effectively promoted the proliferation and migration of human umbilical vein endothelial cells (HUVECs) as well as facilitated the formation of granulation tissue, thereby accelerating wound healing [26]. Inspired by PRP-based osteoarthritis therapy, we further explored the potential of CGF-loaded GM hydrogels to promote cartilage tissue repair [27]. We have further delineated the proliferation and migration of chondrocytes using live/dead staining, CCK-8 assay, and scratch wound healing assay *in vitro* [28]. These hydrogels were further transplanted into a rabbit cartilage defect model *via in situ* gelation. The repaired tissues were comprehensively analyzed using histological and immuno-histochemical staining(Fig. 1).

2. Methods

2.1. Extraction and culture of rabbit chondrocytes

Knee cartilage from lactating rabbits was soaked in dilute iodophor for 10 min, rinsed three times with sterile PBS, and minced into particles with a size of 1 × 1 × 1 mm^3 using ophthalmic scissors. The particles were digested by shaking with three volumes of 0.015 % type II collagenase at 37 °C for 60 min, and then repeatedly pipetted to dissociate cells. The supernatant was filtered through a cell sieve, centrifuged at 1000 rotations per minute (rpm) for 5 min, and the pellets were resuspended in 10 % fetal bovine serum (FBS)-supplemented DMEM-F12 medium. The dissociated cells were first seeded into the culture flasks and then incubated at 37 °C and 5 % CO_2; the medium was replaced after 72 h for subculture.

2.2. Preparation of GM@CGF hydrogel

CGF Extraction: Fresh rabbit blood underwent centrifugation: at 2700 rpm for 2 min, at 2400 rpm for 4 min, at 2700 rpm for 4 min, and at 3000 rpm for 3 min. Thereafter, blood was separated into various layers, separately upper layer of platelet-poor plasma, middle layer of fibrin-rich CGF gel (containing aggregated platelets), and lower layer of erythrocytes (Fig. 2a). The middle layer was collected *via* sterile syringe extrusion to obtain CGF extract and membrane.

To obtain GM hydrogels (GM, EFL-GM-30; Jiangsu, China) precursor solution, 0.05 g lithium phenyl-2,4,6-trimethylbenzoylphosphinate

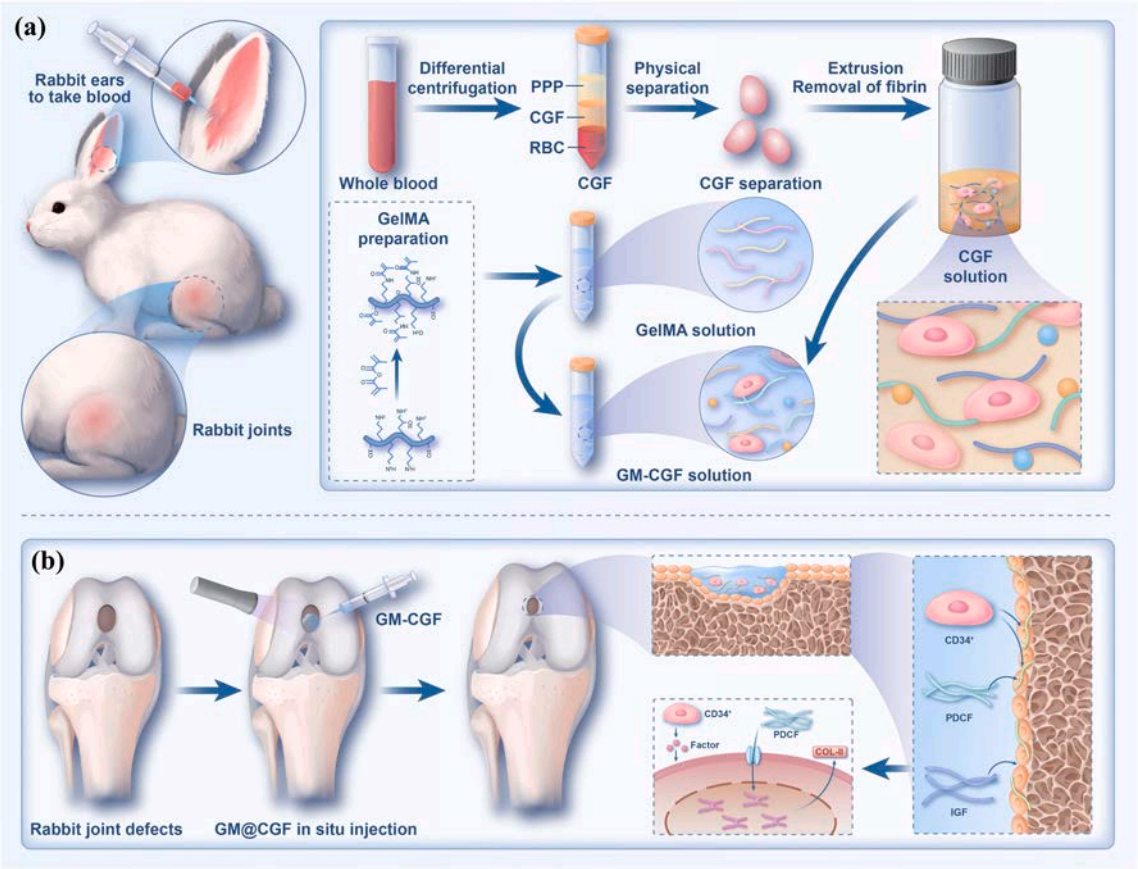

Fig. 1. Summary of the experimental design. (a) Isolation of CGF from whole blood and preparation of GM@CGF scaffolds. (b) Establishment of osteochondral defect model and an illustration about a dynamic and interactive healing process of GM@CGF scaffolds during cartilage regeneration.

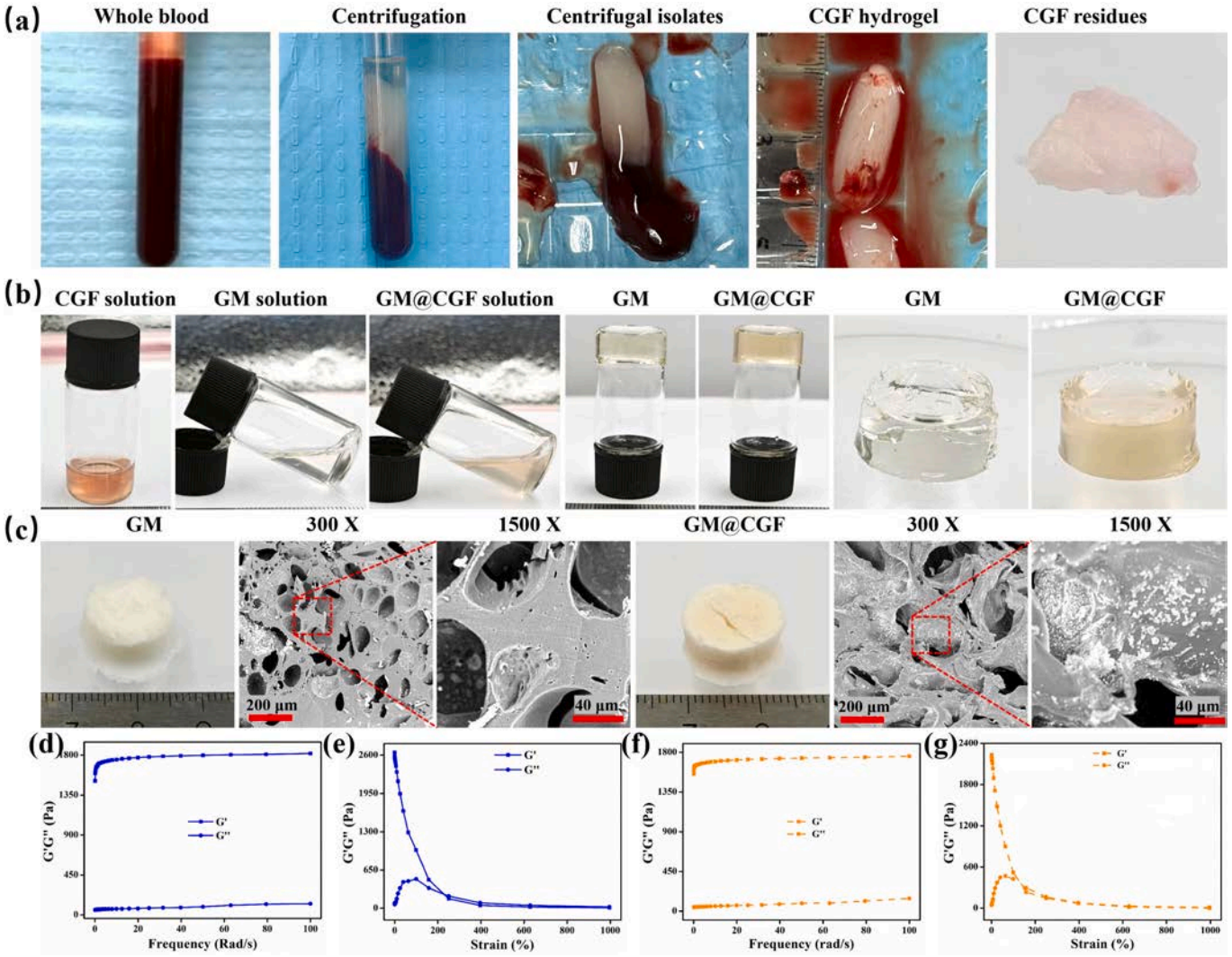

Fig. 2. Preparation and physical characterization of hydrogels. (a) Preparation of CGF by centrifugation from whole blood. (b) Solution of hydrogels were crosslinked by ultraviolet light. (c) Morphological analysis of freeze-dried hydrogels. Rheological analysis of various hydrogels, frequency sweep analysis of GM (d) and GM@CGF (f), strain sweep analysis of GM (e) and GM@CGF (g).

(LAP) was dissolved in 10 mL PBS at 50 °C in a water bath to obtain 0.5 % (*w/v*) LAP solution. 1 g of GM was added into 5 mL of LAP solution, and finally dissolved in a water bath at 50 °C under light protection for 30 min to obtain 20 % (w/v) solution. The precursor solution of GM was diluted as required for subsequent assays.

GM@CGF Hydrogel: GM precursor solution (20 % w/v) and CGF extraction were mixed at a volume-to-volume ratio of 1:1 (mL/mL) to prepare GM@CGF precursor, which was crosslinked with 365 nm ultraviolet (UV) light at 10 mW/cm^{2}for 30–60 s to form the hydrogel [26].

2.3. Characterization of hydrogels

The surface morphology of hydrogel was observed using scanning electron microscope (SEM, Hitachi TM-1000, Japan). The dried samples were mounted onto copper stubs, sputter-coated with gold, and imaged. For degradation analysis, cylindrical hydrogels (200 μL of precursor solution) were soaked into 10 mL PBS with shaking. At pre-defined intervals, samples were lyophilized for morphological analysis with SEM. For mechanical properties, hydrogels (diameter, 10 mm and height, 8 mm, $n = 4$/group) were tested with a universal tensile testing machine (Instron 5567, USA) at a strain rate of 10 mm/min for up to the rupture. Tensile strength was determined from the stress-strain curve. Young's modulus (E) was calculated as a slope of the initial 10 % linear region.

For swelling assay of hydrogels, the original weight of hydrogel discs (Φ = 10 mm, thickness = 3 mm) was recorded as A_0. Afterwards, hydrogel discs were immersed in phosphate-buffered saline (PBS) and the weight was recorded as A_x at various time points. The swelling rate was calculated by Eq. (1):

$$Swelling\ rate = \frac{(A_x - A_0)}{A_0} \times 100\% \quad (1)$$

For degradation assay, hydrogels (Φ = 10 mm, thickness = 3 mm) were blotted dry, lyophilized, and weighed (B_t) at different time points.

Moreover, surface morphology of degraded hydrogels was observed using SEM. The weight of freeze-dried hydrogels was recorded as B_0, and the degradation rate was calculated using Eq. 2:

$$\text{Degradation ratio } (\%) = \frac{(B_0 - Bt)}{B_0} \times 100\% \quad (2)$$

For rheological analysis, hydrogels (φ = 10 mm, height = 5 mm) were analyzed using a rotational rheometer (DHR-3, TA, USA) at 37 °C. Storage modulus (G′) and loss modulus (G″) were recorded at 1.0 % strain over 1–100 rad/s.

2.4. Biocompatibility and biological function assay in vitro

2.4.1. Cytocompatibility in vitro

GM@CGF and GM precursor solutions were added into 24-well plates, crosslinked with UV, and then seeded with rabbit chondrocytes (2×10^4 cells/well). At day 1, 3, and 5, live/dead staining was carried out using 500 μL of staining solution per well at 37 °C for 30 min. Cells were observed using a confocal microscope (green and colours indicate live and dead cells, respectively). Cell proliferation was studied using CCK-8 assay. Hydrogel extracts were prepared by immersing GM@CGF in DMEM-F12 for 24 h. Chondrocytes (1×10^5 cells/well) were firstly seeded in 6-well plates, then treated with the extract solution of different types of hydrogels, and subjected to live/dead staining and CCK-8 assay. Cells were also stained with DAPI/phalloidin staining at day 7.

2.4.2. Scratch wound healing assay in vitro

Chondrocytes (1×10^5 cells/well) were seeded in 6-well plates and grown for up to 90 % confluence. Cells were scratched using a sterile 200 μL pipette tip. Cells were rinsed with PBS and treated with the extract solution of different types of hydrogels. Images were captured at 12 h and 24 h, and the quantitative analysis was performed using Imagine J (NIH, v1.8.0, USA). The migration rate (MR) was calculated using Eq. 3:

$$\mathrm{MR}\ (\%) = \frac{(C_0 - C_t)}{C_0} \times 100\% \tag{3}$$

where C_0 and C_t indicate scratch area at the beginning as well as at 12 h or 24 h.

2.4.3. Transwell migration assay in vitro

Sterile hydrogels ($\Phi = 15$ mm, thickness = 3 mm) were placed into 24-well plates along with 800 μL medium for 4 h. Chondrocytes (3×10^4 cells/well/insert) were added into Transwell inserts. After 24 h, inserts were rinsed with PBS, fixed using 4 % paraformaldehyde (PFA), stained with crystal violet, and observed with a confocal microscope. For quantitative analysis, membranes were treated with 5 % oxalic acid, and optical density (OD) of the resulting solution was measured at 590 nm [27].

2.5. Subcutaneous implantation of hydrogels

This study was approved by the Welfare and Ethics Committee of the Department of Laboratory Animal Science at Army Medical University (AMUWEC20235048). The GM@CGF and GM hydrogels ($\varphi = 10$ mm; thickness = 2 mm) were subcutaneously implanted in Sprague-Dawley (SD) rats (female, seven-week-old) ($n = 5$/group) for 4 weeks. The SD rats were anesthetized with an intra-peritoneal injection of pentobarbital sodium (60 mg/mL). At 2 w and 4 w, the implants with surrounding tissues were harvested, fixed with 4 % PFA, and sectioned for Hematoxylin and Eosin (H&E) staining and Masson's trichrome (MT) staining.

When observing new capillaries in tissue sections using H&E staining, first the junction between the hydrogel and the tissue was located under a low-power microscope. Thereafter, imaging was performed at a high-power: New capillaries typically present small and irregular lumens, either containing only a few number of red blood cells (RBC) or none. The edge of the lumen shows a single layer of flattened or cuboidal endothelial cells (ECs) arranged in a monolayer, with blue-purple round or oval nuclei (adherent nuclei) and a high nucleocytoplasmic ratio. They are often accompanied by fibroblasts, inflammatory cells, and loose granulation tissue in the surrounding area. Five random fields of view (200 × magnification) were selected from each section. The number of new capillaries was counted using ImageJ software ($n = 6$ per group).

2.6. Rabbit cartilage repair in vivo

New Zealand rabbits were anesthetized with 3 % sodium pentobarbital at the ear margins (dose, 30 mg/kg IV). Knee joints were disinfected and incised, and then the joint capsule was opened to expose the femoral trochlea. A 3 mm × 2 mm (diameter × depth) osteochondral defect was created using a trephine. There were three groups: blank (untreated), GM (*in situ* crosslinked), and GM@CGF (*in situ* crosslinked). After surgery, joints were sutured, and rabbits received cefuroxime sodium (0.5 g/rabbit IV) for infection prophylaxis. Rabbits were euthanized at 4 w and 12 w; femurs were harvested for analysis. Detailed methods of gross scoring, imaging, and histological examination are described in supporting information.

2.7. Statistical analysis

All data were collected from at least three independent samples and quantitative data was expressed as mean ± standard deviation (SD). The normally distributed data were analyzed using *t*-tests or one-way ANOVA followed by Tukey's post-hoc test. The skewed data were analyzed by rank sum test. Significance was defined as $^*P < 0.05$, $^{**}P < 0.01$, $^{***}P < 0.001$.

3. Results and discussion

3.1. Characterization of GM@CGF hydrogel

We successfully prepared GM@CGF hydrogels by blending appropriate proportions of CGF extract and GM solution. CGF is derived from blood using continuous gradient centrifugation, which is primarily composed of different types of components, including fibrin, platelets, growth factors, leukocytes, and $CD34^+$ cells. CGF extract exhibits a light red colour, in part, due to a few numbers of ruptured red blood cells (RBCs). Upon UV crosslinking, the GM hydrogel appeared to be transparent, while the GM@CGF hydrogel exhibited a light pink colour (Fig. 2b). Both the lyophilized GM hydrogel and GM@CGF hydrogel exhibited a loose porous 3D structure, which can facilitate the release of growth factors from the GM@CGF hydrogel, and may also serve as a scaffold for cell growth, thereby promoting the in-growth of chondrocytes (Fig. 2c). Moreover, rheological analysis, including strain change and frequency sweep displayed insignificant influence of CGF on the mechanical properties of GM hydrogels (Fig. 2d-g). The appropriate mechanical properties may help maintain the integrity of the hydrogel scaffold and support cell adhesion and proliferation.

Compression tests revealed that hydrogels can withstand 50 % strain (Fig. 3a). The inclusion of CGF into GM hydrogels reduced mechanical strength (Young's modulus:GM, 62.6 ± 4.0 kPa and GM@CGF, 56.5 ± 4.3 kPa; maximum compressive strength: GM, 233.8 ± 14.0 kPa and GM@CGF, 119.9 ± 13.5 kPa) (Fig. 3c-d). While the incorporation of CGF into GM hydrogels can enhance the bioactivity of GM/CGF hydrogels, the fibrin component of CGF may disrupt the photo-crosslinked network of GM, thereby causing a significant reduction in Young's modulus and compressive strength. On one hand, moderate softening of mechanical properties may closely mimic the flexibility of native cartilage, thereby reducing the stress shielding effect and promoting cell response to mechanical signals. Nonetheless, insufficient mechanical support may lead to premature collapse or deformation of the hydrogel under joint dynamic load, which may hinder the structural stability of the defect area, adversely influence mechanical functional maturation of the neocartilage, and may even induce mechanical mismatch between repaired tissue and surrounding normal cartilage tissues, thereby increasing secondary injury risks.

The swelling efficiency of GM@CGF hydrogels was higher than that of the GM hydrogels (GM@CGF, 10.9 ± 7.8 % and GM, 7.78 ± 0.95 %) as evaluated at 24 h. Higher swelling efficiency of GM@CGF may be ascribed to high porosity and larger pore size than that of the GM

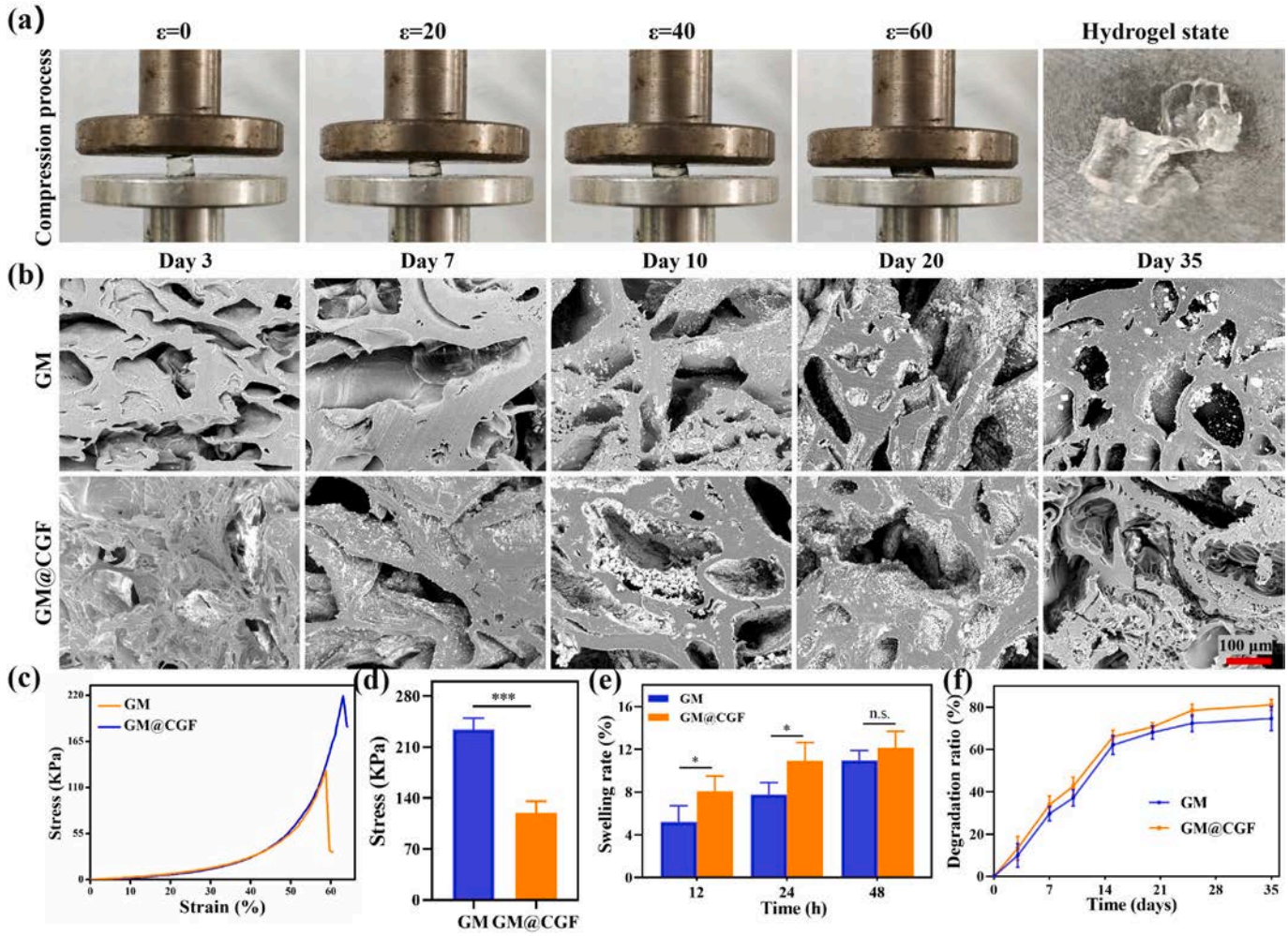

Fig. 3. Mechanical properties and degradation of hydrogels. (a) Schematic diagram illustrating mechanical testing of hydrogels. (b) Morphological analysis of freeze-dried hydrogels after degradation *in vitro* for up to 35 days. (c) Representative compressive stress-strain curves. (d) compressive strength of hydrogels. (e) Hydrogel swelling at various time points. (f) Degradation of hydrogels. $^{*}P < 0.05$, $^{***}P < 0.001$.

hydrogels (Fig. 3e). Consequently, GM@CGF hydrogels could absorb a large amount of liquid in a shorter time period and attain swelling equilibrium. GM@CGF hydrogels also displayed higher degradation than that of the GM hydrogels, which may have implications for the gradual release of growth factors (35d, GM@CGF, 81.1 ± 3.3 % and GM, 74.7 ± 4.9 %) (Fig. 3f). However, upon hydrogel degradation *in vitro*, there was an insignificant difference between GM hydrogel and GM@CGF hydrogels in terms of the morphology, which is likely due to the longer degradation cycles, indicating that the degradation might have occurred progressively in an out-to-in form with minimal morphological changes (Fig. 3b).

Concerning the correlation between the release kinetics of growth factors, such as TGF-β and VEGF in CGF and tissue repair, our previous report indicated that GM@CGF hydrogel can attain release equilibrium of growth factors after 6 h. The cumulative release rates were 74.4 ± 2.1 %, 76.0 ± 2.3 %, and 70.9 ± 3.2 % for EGF, PDGF, and TGF-β1, respectively. On the other hand, by 72 h the cumulative release rates of EGF, PDGF, and TGF-β1 were found to be 80.5 ± 1.5 %, 87.3 ± 2.2 %, and 78.1 ± 4.6 %, which correspond to the final concentrations of 197.44 ± 13.72 pg/mL, 225.59 ± 28.29 pg/mL, and 154.35 ± 23.06 pg/mL, respectively [26]. These data revealed the rapid release of growth factors from GM@CGF hydrogel at initial time points, which can help achieve an effective concentration of growth factors in a shorter time period after hydrogel implantation. Once attained release equilibrium, the growth factors remained at a suitable concentration.

3.2. Biocompatibility and bioactivity of hydrogels in vitro

The cytocompatibility of the hydrogel was demonstrated by assessing the viability and proliferation of chondrocytes, as evidenced by the successful cell-material interactions observed *in vitro*. We initially observed the proliferative activity of chondrocytes on culture plate using extract solution from GM and GM@CGF hydrogels. Live/dead staining and phalloidin staining revealed negligible differences in cell viability and cell morphology between GM and GM@CGF groups (Fig. 4a-b). However, the CCK-8 assay indicated enhanced cell proliferative activity at day 7, suggesting that GM@CGF hydrogels were cytocompatible *in vitro* (Fig. 4d).

Moreover, we inoculated rabbit articular chondrocytes on the surface of hydrogels. Live/dead staining showed normal morphology of chondrocytes seeded on the surface of GM@CGF hydrogel; chondrocytes exhibited intact cell membranes and regular cell morphology (Fig. 4c). At day 5, the fluorescence intensity of cells in the GM@CGF hydrogel group was lower than that of the control group (Fig. S1). However, CCK-8 assay showed higher OD value of cells in the GM@CGF hydrogels as compared to the GM hydrogels (OD values: GM, 1.30 ± 0.04 and GM@CGF, 1.58 ± 0.05) (Fig. 4e). Higher cell proliferation in GM@CGF hydrogel may be ascribed to its ability to form 3D scaffold and enhance cellular infiltration and proliferation, along with the release of growth factors for subsequent cell proliferation [29–31].

The Safranin O staining of chondrocytes revealed that the CGF can

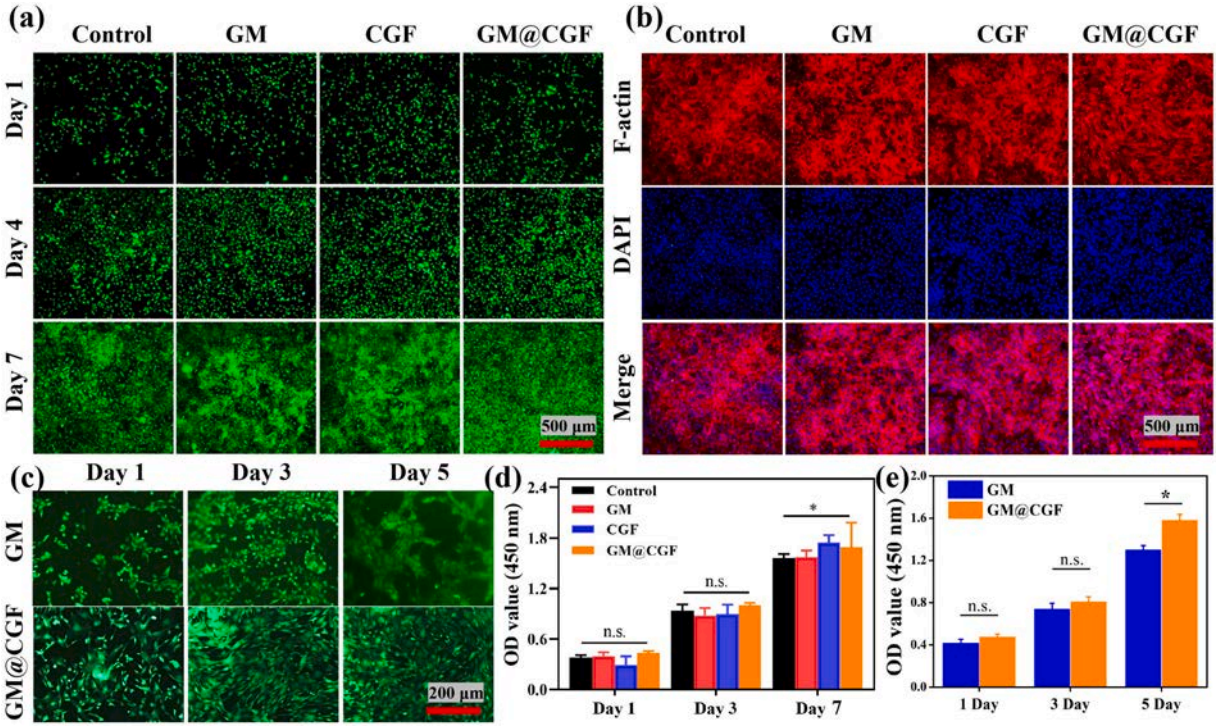

Fig. 4. *In vitro* biocompatibility of hydrogels. Live/dead staining (a), phalloidin staining (b) and CCK-8 assay (d) of chondrocytes at day 1, 4, and 7 after incubation with the extract solution of GM and GM@CGF. Live/dead staining (c), and CCK-8 assay (e) of chondrocytes at 1d, 3d, and 5d after inoculation on the hydrogel surface. $^{*}P < 0.05$.

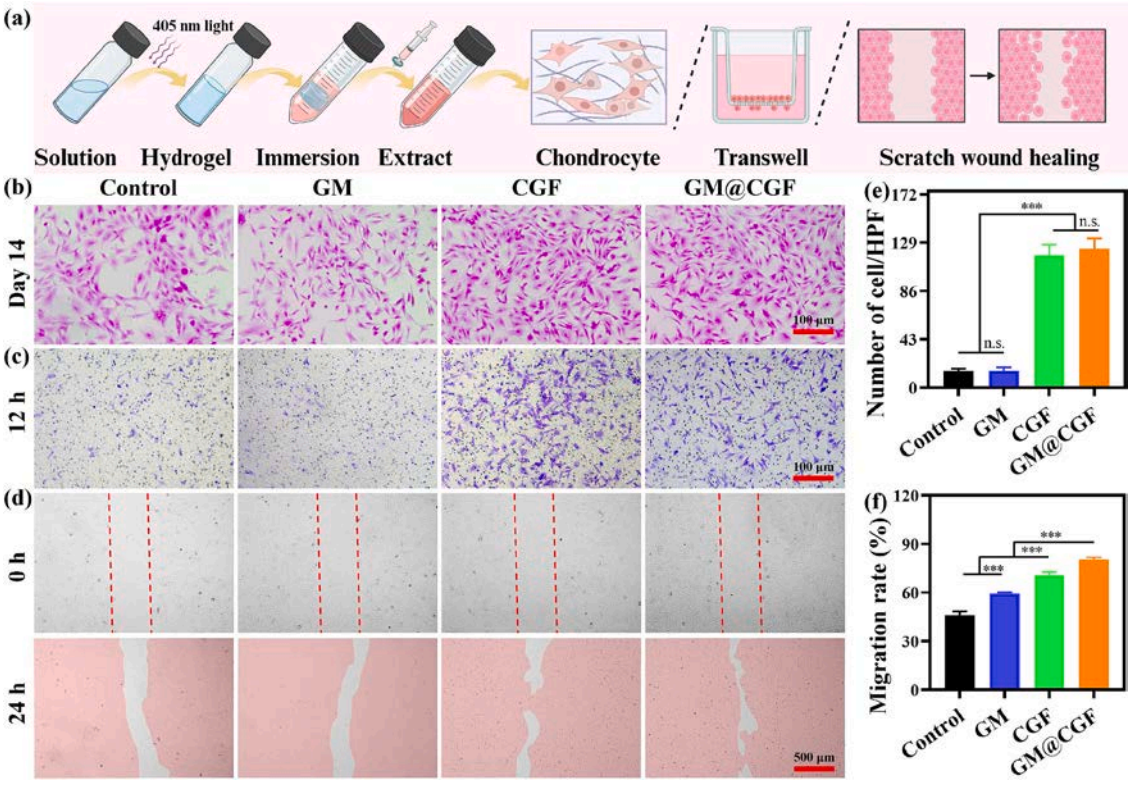

Fig. 5. *In vitro* bioactivity of hydrogels. (a) Schematic representation of Transwell migration assay and scratch wound healing assay. (b) Safranin O staining of chondrocytes at day 14. (c) Representative images of the migration of chondrocytes in an Transwell migration assay at 12 h *in vitro*. (d) Representative images from a scratch wound healing assay at 24 h. (e) Number of migrated cells/HPF in a Transwell migration assay. (f) Cell migration rate in a scratch wound healing assay, $^{***}P < 0.001$.

promote chondrocyte matrix secretion (Fig. 5b). Moreover, the chemotactic effect of GM@CGF hydrogel was ascertained by scratch wound healing assay *in vitro*. As shown in Fig. 5d, there was almost identical wound depth at $t = 0$ h, which became smaller in CGF and GM@CGF groups at 24 h. The percentage wound closure was found to be 46.0 ± 2.0 %, 55.4 ± 0.8 %, 70.7 ± 1.6 %, and 80.3 ± 1.1 % for control, GM, CGF, and GM@CGF groups, respectively (Fig. 5f). The migration of articular chondrocytes was assessed by Transwell migration assay. By 12 h, the numbers of migrated cells were found to be 15.5 ± 1.6, 16.1 ± 2.5, 118.0 ± 7.5, and 124.0 ± 7.4 for control, GM, CGF, and GM@CGF group, respectively (Fig. 5c & 5e). In respect of PDGF isoforms, PDGF-AB exhibited the strongest chemotactic effect, and increased the chemotactic activity of chondrocytes in the superficial zone [32]. These results show that CGF exhibits an ability to promote the migration of chondrocytes, which may also have implications for the cytocompatibility of GM@CGF hydrogels.

3.3. In vivo biocompatibility

To delineate the degradation of hydrogel *in vivo*, we subcutaneously implanted them in rats (Fig. 6a). H&E and MT stainings revealed a distinct change in the structural integrity of GM and GM@CGF hydrogels, which was accompanied by the considerable accumulation of inflammatory cells in the surrounding tissues 2 weeks post-operatively. GM@CGF hydrogel was significantly degraded with only a few residual gel fragments. Neutrophils, macrophages, fibroblasts, and lymphocytes were infiltrated into the GM@CGF hydrogel. Moreover, a large number of new capillaries and dense arrangement of collagen fibers could be observed in the inner side of GM@CGF hydrogel at week 4 post-operatively. Conversely, GM hydrogels displayed poor degradability with fewer cell infiltration, minimal collagen deposition, and only a few numbers of new capillaries (Fig. 6b). These results indicate that GM@CGF hydrogel can be rapidly degraded *in vivo*, which may also have implications for the release of different types of growth factors for tissue repair. These released growth factors can promote the migration, proliferation and differentiation of different types of cells, such as fibroblasts, neutrophils, and smooth muscle cells (SMCs); these cells may further promote hydrogel degradation.

Though we observed higher immune cell infiltration iwith CGF implantation, including neutrophils and monocytes with CGF implantation, we did not carry out an in-depth elucidation of macrophages phenotype as well as M1/M2 macrophages ratio. Moreover, we did not analyze the content of immune-regulatory markers, including Arg-1, iNOS, IL-10. Consequently, it yet remains to be deciphered if CGF can mediate the regenerative effects of macrophages by regulating their polarization. It is also worth to note that the biocompatibility of hydrogels was discerned using rabbit-derived CGF in a rat subcutaneous implantation model, the xenogenicity may have induced a mild immune response, as indicated by the more numbers of infiltrated immune cells . Nevertheless, this response was transien, which may not impair the biocompatibility of hydrogels in the long-term. In our future studies, we will study the effect of autologous CGF in a rabbit subcutaneous model to obviate this limitation.

3.4. Cartilage repair of GM@CGF hydrogel

To further evaluate the efficacy of hydrogels for cartilage tissue repair, osteochondral defects (diameter, 3 mm and depth, 2 mm) were established. An *in-situ* hydrogel was then applied to the defect site to promote the healing process (Fig. 7a). Fig. 7b presented macroscopic images of articular heads harvested at week 4 and week 12 post-implantation of hydrogels. At week 4, both the GM@CGF and GM hydrogel groups exhibited milky-white colour alongside slightly firm regenerated tissues. These hydrogels displayed by grade II reddish

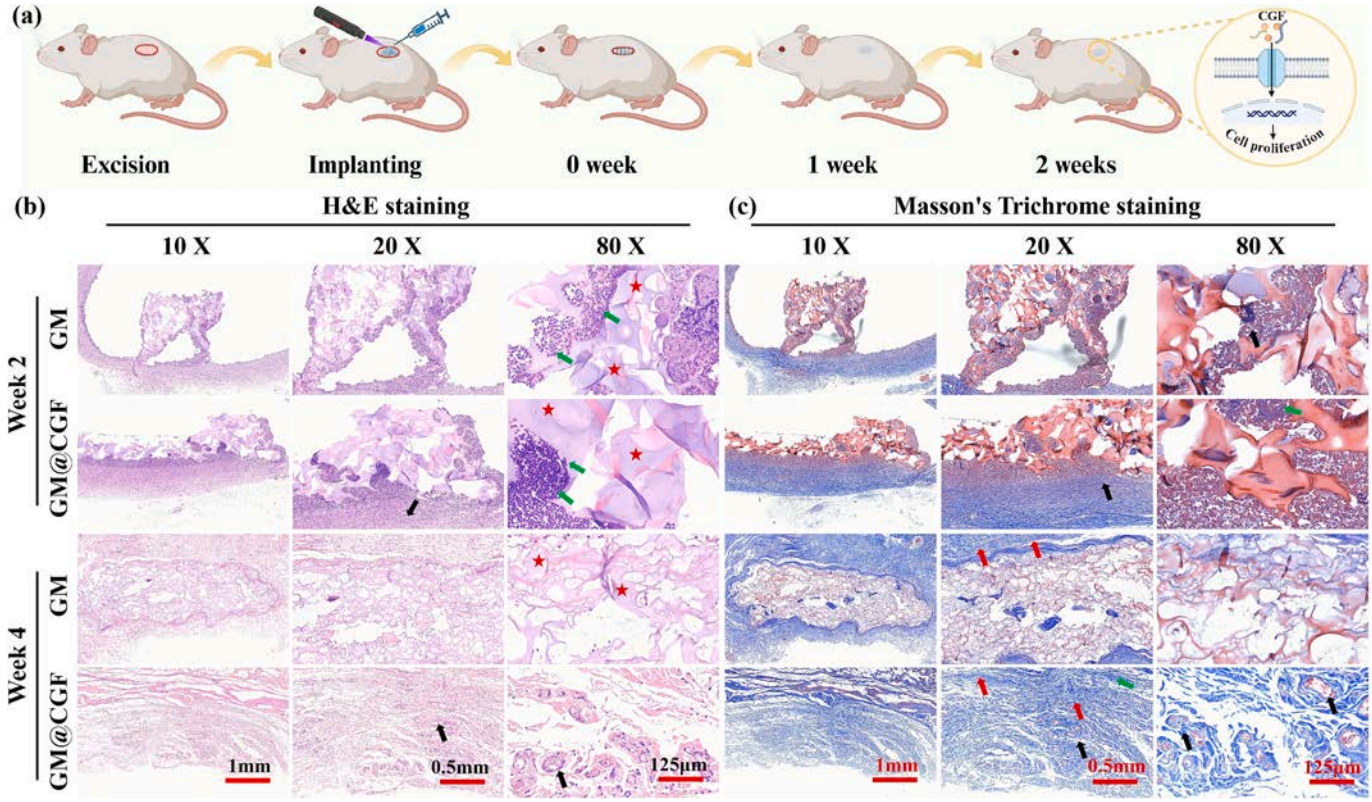

Fig. 6. Evaluation of biocompatibility *in vivo*. (a) Subcutaneous implantation of hydrogels in rats. (b) H&E staining and MT staining of hydrogels along with the surrounding tissues. The green arrow, red arrow, black arrow and red five-pointed star indicated the inflammatory cells, collagen fibers, new capillaries and gel fragments, respectively. (For interpretation of the references to colour in this figure legend, the reader is referred to the web version of this article.)

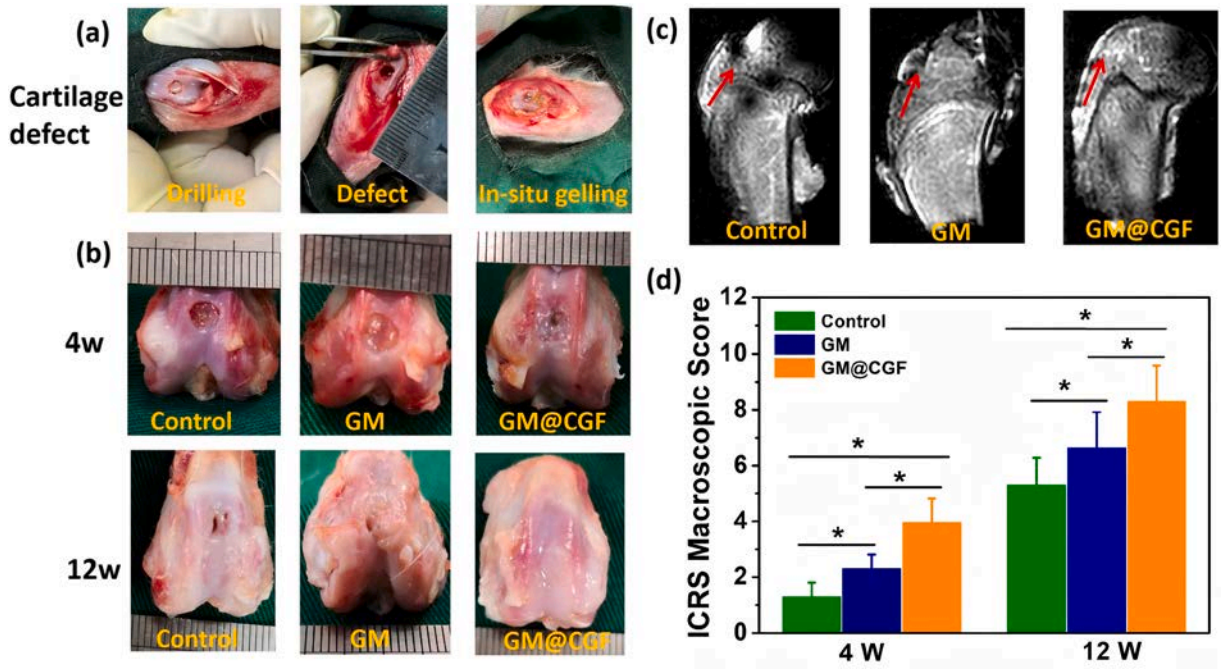

Fig. 7. Evaluation of cartilage repair effect of different types of hydrogels in a rabbit cartilage defect model *in vivo*. (a) Schematic illustration of the creation of a rabbit cartilage defect model. Representative images of macroscopic effect of cartilage repair (b) and ICRS scores (d) of the three groups at 4 and 12 weeks post-operatively. (c) Micro-MRI evaluation of cartilage repair. Red arrows indicate the defect site. $^{*}P < 0.05$. (For interpretation of the references to colour in this figure legend, the reader is referred to the web version of this article.)

regenerated tissue albeit irregular tissue surface. By week 12, GM@CGF group displayed neotissue regeneration accompanied by a smooth surface and indistinct boundary with the surrounding tissues, thereby mimicking the morphological features of adjacent hyaline cartilage. In contrast, the GM hydrogel group showed irregularly-shaped regenerated tissue protruding above the joint surface with a clear demarcation from normal cartilage. The control group lacked full defect filling, and it additionally displayed distinct central cavities.

Quantitative analysis by ICRS score further confirmed these macroscopic observations. By week 4, ICRS scores were 4.11 ± 0.82 (GM@CGF hydrogel), 2.33 ± 0.48 (GM hydrogel), and 1.43 ± 0.47 (control). By week 12, ICRS scores became 8.33 ± 1.24, 6.46 ± 1.24, and 5.33 ± 0.94 for GM@CGF, GM, and control groups, respectively (Fig. 7d), which were in consistence with the macroscopic findings. We also observed significant improvement in terms of defect filling, collagen deposition, and integration between regenerated and native cartilage with an increase in the implantation period, thereby highlighting the potential of hydrogels to promote cartilage tissue repair. GM@CGF hydrogel group outperformed other groups in terms of macroscopic appearance at both time points, in part, due to its ability to provide the 3D structural support and bioactive growth factor delivery [31–34]. Micro-MRI analysis revealed smooth, continuous distal femoral cartilage regeneration with slightly elevated subchondral signals (predominantly grade I-II) in GM@CGF hydrogel group. On the other hand, GM hydrogel and control groups showed discontinuous cartilage layers with persistent defects (primarily grade III) (Fig. 7c).

Three groups of knee cartilage injury specimens at week 12 were further subjected to H&E staining and safranin O-fast green staining. H&E staining showed no evident cartilage repair in the control group, where only irregular fibrous tissue filled the injured surface. There were only a few chondrocytes and subchondral bone was found to be in a remodeling state. In the GM hydrogel group, fibrocartilage tissue dominated the defect area, showing more extensive filling than that of the control group. Nevertheless, the repaired region lacked a distinct hierarchical structure of chondrocytes; cells were mainly arranged in a disorganized pattern. The GM@CGF hydrogel group exhibited distinct hyaline cartilage regeneration interspersed with fibrocartilaginous tissue at the injury site, where a subset of chondrocytes were clustered in columnar-like arrangements, roughly recapitulating the layered structure of native cartilage.

Although subchondral bone tissue remained mostly intact, the interface with adjacent normal cartilage displayed an irregularity. Since Safranin O specifically binds to chondroitin sulfate and keratan sulfate, the intensity of Safranin O-fast green staining approximately correlates with the concentration of these anionic glycosaminoglycans, thereby reflecting the content of proteoglycans as well as their distribution in the matrix. The GM@CGF hydrogel group showed well-formed hyaline cartilage, radial chondrocyte columns in the deep cartilage layer, and closed bone plates. In contrast, the GM hydrogel group demonstrated suboptimal outcomes, with regenerated cartilage dominated by less mature fibrous microstructures and significantly reduced new bone growth reaching the trochlear bone plate level.

The control group performed poorly, though residual granulation tissues were still detectable (Fig. 8a). The combined application of growth factors, cells and scaffolds has emerged as a recent research focus to facilitate defect healing. Sun et al. loaded bone marrow mesenchymal stem cells (BMSCs) in growth differentiation factor 5 (GDF5)-conjugated 3D scaffolds. BMSCs-loaded scaffolds showed enhanced cartilage tissue repair as compared to the control group [35]. Similarly, Singh et al. incorporated PRP/sodium alginate (SA) into 3D scaffolds comprised of chitosan, chondroitin sulfate, and silk fibroin. These scaffolds enabled higher glycosaminoglycan deposition, enhanced metabolic activity, enhanced collagen type II (Col II) and aggrecan expression, and significant cartilage regeneration [36]. Moreover, hematopoietic stem cells (HSCs) in CGF hydrogel may participate in cartilage regeneration presumably *via* their direct differentiation into chondrocytes, which can be further enhanced by the induction of growth factors (high-content components in CGF gel) as well as immunomodulatory effects. Besides, HSCs can secrete more anti-inflammatory factors. In addition, endothelial progenitor cells (EPCs) can promote angiogenesis around the injury area to improve local blood supply as well as provide nutritional support for cartilage tissue repair. To put together, HSCs and EPCs can

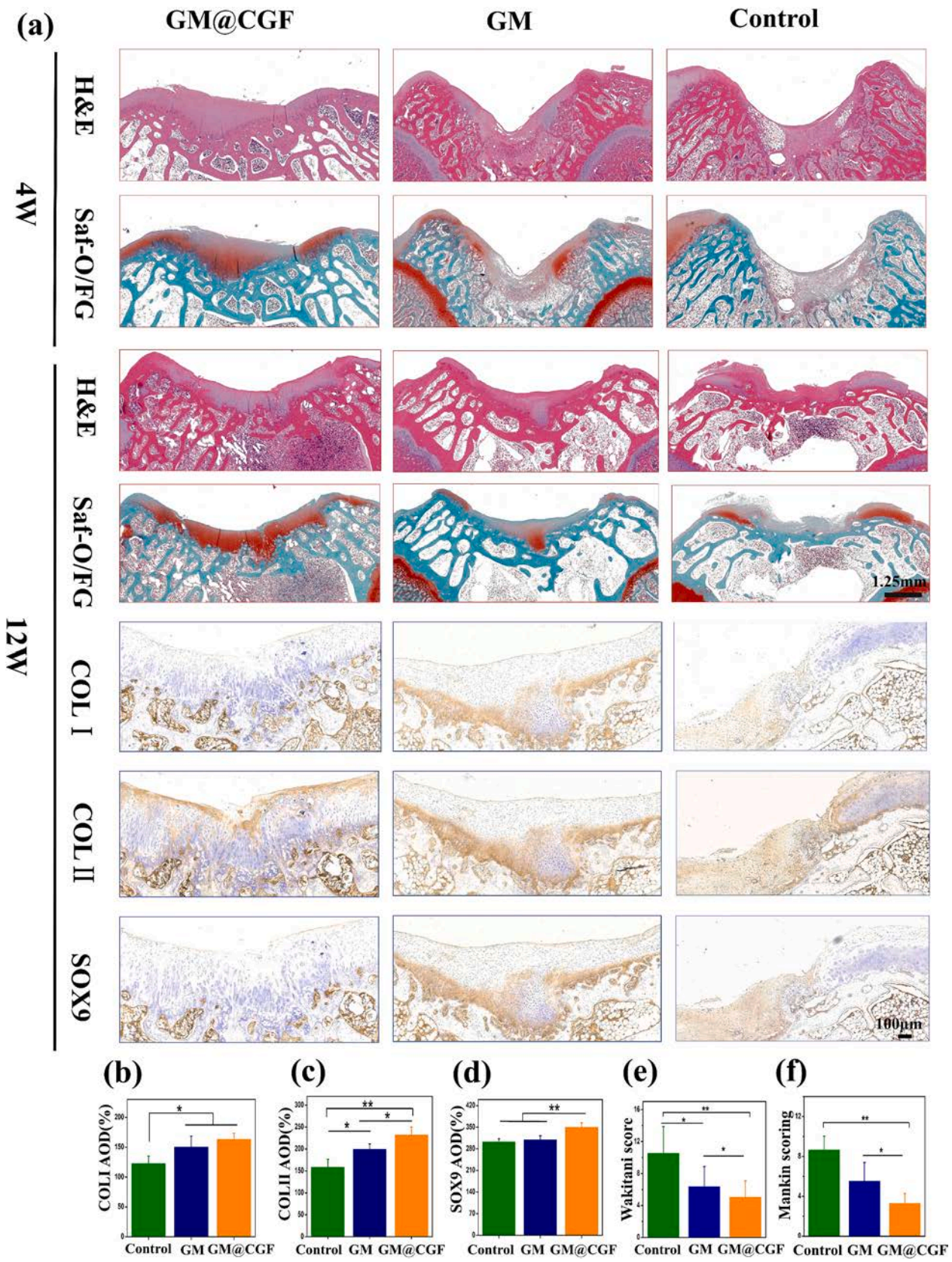

Fig. 8. Histological evaluation of cartilage repair effect: (a) Safranin O-fast green staining, H&E staining, and immunohistochemical staining (COL I, COL II, and SOX9) of articular cartilage at 4 and 12 weeks post-operatively; (b-d) average optical density of COL I, COL II, and SOX9; (e) Wakitani score; (f) Mankin rating. $^{*}P < 0.05$, $^{**}P < 0.01$. (For interpretation of the references to colour in this figure legend, the reader is referred to the web version of this article.)

synergistically act with growth factors *via* paracrine effects and prolonged action time.

We carried out histological analysis using Wakitani cartilage repair scoring system and a modified Mankin scoring system. It is worth to note that higher scores indicate poor tissue regeneration outcome. GM@CGF hydrogel group achieved the most significant repair improvement (Wakitani score, 5.17 ± 1.92 and Mankin score, 3.38 ± 0.92), which was followed by GM hydrogel group (Wakitani score, 6.50 ± 2.38 and Mankin score, 5.63 ± 1.77), and the control group (Wakitani score, 10.66 ± 3.21 and Mankin score, 8.72 ± 1.26) (Fig. 8e & 8f). Therefore, GM@CGF hydrogel outperformed other groups for cartilage tissue repair, in part, due their ability to enable sustained and controlled release of different types of growth factors, such as VEGF, PDGF, TGF-β. Consequently, this established growth factor reservoir may initiate tissue repair process as well as stimulate the proliferation, migration, and differentiation of chondrocytes/BMSCs. In addition, GM hydrogel may provide a moist microenvironment and ECM-mimicking structure to guide the migration of chondrocytes into the defect site, thereby accelerating repair. [26,34].

COL II and proteoglycans are the primary components of the cartilage ECM. Immunohistochemical staining revealed that the GM@CGF group exhibited the highest AOD values for both COL II and SOX9. Specifically, the AOD values of COL II in the control, GM, and GM@CGF groups were 159.6 ± 15.1 %, 200.6 ± 11.2 %, and 232.9 ± 17.2 %, respectively. Meanwhile, the AOD values of SOX9 were 303.9 ± 8.7 %, 310.7 ± 12.0 %, and 351.8 ± 12.5 % for control, GM, and GM@CGF groups, respectively (Fig. 8b-d). SOX9 is a key transcription factor, which plays a pivotal role in chondrocyte differentiation and cartilage formation. SOX9 can bind with intron splicing site within the high-mobility group (HMG) domain of DNA, thereby activating the expression of COL II and other chondrogenic factors [37]. Similarly, TGF-β can promote the migration, accumulation, proliferation, and differentiation of BMSCs, thereby maintaining chondrocytes phenotype as well as regulating ECM synthesis of chondrocytes [38].

Moreover, TGF-β can activate nuclear SOX9 transcription factor through the TGF-β/Smad signaling pathway and promote the differentiation of BMSCs into chondrocytes [39]. EGF signaling pathway acts as a critical histiocytic regulatory factor. Indeed, EGFR deficiency has been shown to alter cartilage growth plate development in mice, impair chondrocyte survival, and delay endochondral osteogenesis. Phosphorylated EGFR is primarily localized in the superficial layer of articular cartilage, indicating that the EGF signaling pathway plays an important role in maintaining the functional and mechanical properties of superficial articular cartilage [40].

Our study also has some limitations. We did not elucidate biomechanical properties of regenerated cartilage. Besides, we did not elucidate the mechanism underlying CGF-mediated cartilage tissue repair (*e.g.*, through inducing inflammatory cell infiltration or stem cell recruitment). It is also warranted to further exploit proteomics and gene sequencing technologies to investigate the molecular mechanisms driving CGF-mediated cartilage tissue repair. Moreover, we did not compare our results with other bioactive cues-based therapies (*e.g.*, PRP, PRF, *etc.*) or existing clinical treatment methods for cartilage tissue repair, which may obscure the potential of GM@CGFs to induce cartilage tissue repair. In our future studies, we intend to investigate novel nanomaterials for targeted delivery of CGF to enhance the *in vivo* application of CGF while enhancing its adhesion to cartilage tissue [41–43].

4. Conclusion

We successfully fabricated an injectable CGF-loaded gelatin hydrogels, which displayed a porous 3D architecture, good cytocompatibility, and costimulatory properties. The developed hydrogel also facilitated the proliferation, migration, and matrix secretion of chondrocytes *in vitro*. Once implanted in a rabbit cartilage defect model *in vivo*, GM@CGF hydrogels improved the repair efficacy, which was characterized by the formation of reparative tissue with high expression of COL II and SOX9. The GM@CGF hydrogel achieves synergy between sustained growth factor release and structural support, thereby providing a "structure-function" dual-optimization strategy for cartilage regeneration. This innovation further facilitates the clinical translation of autologous biomaterials in the repair of cartilage injuries.

Supplementary data to this article can be found online at https://doi.org/10.1016/j.ijbiomac.2025.147940.

CRediT authorship contribution statement

Xiaoyan Zeng: Writing – original draft, Validation, Investigation. **Lixiang Zhang:** Writing – original draft, Validation, Investigation. **Zewen Wang:** Writing – original draft, Validation, Investigation. **Piming Nie:** Validation, Investigation, Data curation. **Zhengchao Yuan:** Validation, Investigation, Data curation. **Xiumei Mo:** Supervision, Conceptualization. **Chenhui Cai:** Validation, Data curation. **Chao Zhang:** Writing – review & editing, Funding acquisition, Conceptualization. **Yuan Xu:** Writing – review & editing, Supervision, Project administration, Funding acquisition, Conceptualization.

Declaration of competing interest

The authors declare that they have no known competing financial interests or personal relationships that could have appeared to influence the work reported in this paper.

Acknowledgements

This study was partially supported by the grants from Young Doctoral Talent Incubation Program of the Second Affiliated Hospital of the Army Medical University (2023YQB002) and Science and Technology Research Program of Chongqing Municipal Education Commission (KJZD-K202412807). Thanks for http://www.home-for-researchers.com for creating Fig. 1.

Data availability

Data will be made available on request.

References

[1] C. Shen, J. Wang, G. Li, S. Hao, Y. Wu, P. Song, Y. Han, M. Li, G. Wang, K. Xu, H. Zhang, X. Ren, Y. Jing, R. Yang, Z. Geng, J. Su, Boosting cartilage repair with silk fibroin-DNA hydrogel-based cartilage organoid precursor, Bioactive materials. 35 (2024) 429–444.
[2] V.J. Thomas, N.F. Buchweitz, J.J. Baek, Y. Wu, J.J. Mercuri, The development of a nucleus pulposus-derived cartilage analog scaffold for chondral repair and regeneration, J. Biomed. Mater. Res. A 112 (3) (2023) 421–435.
[3] F. Ramzan, A. Salim, I. Khan, Osteochondral tissue engineering dilemma: scaffolding trends in regenerative medicine, Stem Cell Rev. Rep. 19 (6) (2023) 1615–1634.
[4] Y. Campos, A. Almirall, G. Fuentes, H.L. Bloem, E.L. Kaijzel, L.J. Cruz, Tissue engineering: an alternative to repair cartilage, Tissue Eng. Part B Rev. 25 (4) (2019) 357–373.
[5] M. Chen, Z. Jiang, X. Zou, X. You, Z. Cai, J. Huang, Advancements in tissue engineering for articular cartilage regeneration, Heliyon 10 (3) (2024) e25400.
[6] V.C. Carriero, L. Di Muzio, S. Petralito, M.A. Casadei, P. Paolicelli, Cryogel scaffolds for tissue-engineering: advances and challenges for effective bone and cartilage regeneration, Gels 9 (12) (2023).
[7] L. Sun, H. Niu, Y. Wu, S. Dong, X. Li, B.Y.S. Kim, C. Liu, Y. Ma, W. Jiang, Y. Yuan, Bio-integrated scaffold facilitates large bone regeneration dominated by endochondral ossification, Bioactive materials 35 (2024) 208–227.
[8] D. Wu, J. Li, C. Wang, Z. Su, H. Su, Y. Chen, B. Yu, Injectable silk fibroin peptide nanofiber hydrogel composite scaffolds for cartilage regeneration, Mater Today Bio. 25 (2024) 100962.
[9] S. Roszkowski, Therapeutic potential of mesenchymal stem cell-derived exosomes for regenerative medicine applications, Clin. Exp. Med. 24 (1) (2024) 46.
[10] J.H. Lee, P.Y. Kim, Y.C. Pyun, J. Park, T.W. Kang, J.S. Seo, D.H. Lee, G. Khang, Cartilage regeneration using transforming growth factor-beta 3-loaded injectable crosslinked hyaluronic acid hydrogel, Biomater. Sci. 12 (2) (2023) 479–494.

[11] R.A.G. Franco, E. McKenna, M.S. Shajib, B. Guillesser, P.G. Robey, R.W. Crawford, M.R. Doran, K. Futrega, Microtissue culture provides clarity on the relative chondrogenic and hypertrophic response of bone-marrow-derived stromal cells to TGF-β1, BMP-2, and GDF-5, Cells 13 (1) (2023).
[12] H. Zhao, Z. Zhao, D. Li, X. Wang, D. Dai, H. Fu, Effect study of exosomes derived from platelet-rich plasma in the treatment of knee cartilage defects in rats, J. Orthop. Surg. Res. 18 (1) (2023) 160.
[13] L. Zhou, V.O. Gjvm, J. Malda, M.J. Stoddart, Y. Lai, R.G. Richards, K. Ki-Wai Ho, L. Qin, Innovative tissue-engineered strategies for osteochondral defect repair and regeneration: current progress and challenges, Adv. Healthc. Mater. 9 (23) (2020) e2001008.
[14] A. Puiggalí-Jou, M. Asadikorayem, K. Maniura-Weber, M. Zenobi-Wong, Growth factor-loaded sulfated microislands in granular hydrogels promote hMSCs migration and chondrogenic differentiation, Acta Biomater. 166 (2023) 69–84.
[15] Z. Zhou, J. Wang, C. Jiang, K. Xu, T. Xu, X. Yu, J. Fang, Y. Yang, X. Dai, Advances in hydrogels for Meniscus tissue engineering: a focus on biomaterials, crosslinking, Therapeutic Additives, Gels. 10 (2) (2024).
[16] Y. Li, S. Liu, J. Zhang, Y. Wang, H. Lu, Y. Zhang, G. Song, F. Niu, Y. Shen, A. C. Midgley, W. Li, D. Kong, M. Zhu, Elastic porous microspheres/extracellular matrix hydrogel injectable composites releasing dual bio-factors enable tissue regeneration, Nat. Commun. 15 (1) (2024) 1377.
[17] H. Tang, W. Sun, X. Liu, Q. Gao, Y. Chen, C. Xie, W. Lin, J. Chen, L. Wang, Z. Fan, L. Zhang, Y. Ren, Y. She, Y. He, C. Chen, A bioengineered trachea-like structure improves survival in a rabbit tracheal defect model, Sci. Transl. Med. 15 (714) (2023) eabo4272.
[18] Y. Chen, H. Tang, Y. Zhang, L. Wang, J. Zhu, L. Wang, A. Li, X. Zeng, B. Yin, Y. Liang, X. Dong, Q. Bai, Z. Pan, L. Wang, L. Zhang, M. Yang, Y. She, W. Sun, K. Zhang, C. Chen, Multiplexed self-adaptable Janus hydrogels rescue epithelial malfunction to promote complete trachea repair, Nat. Commun. 16 (1) (2025) 5734.
[19] Q. Bai, H. Tang, Y. Chen, Z. Pan, W. Lin, L. Wang, Y. Hu, B. Xu, M. Yang, G. Zhao, W. Sun, Y. He, C. Chen, Modular strategy with autologous bioreactor: a potential way for organ engineering, International Journal of Extreme Manufacturing. 7 (2) (2025) 022001.
[20] F. Tabatabaei, Z. Aghamohammadi, L. Tayebi, In vitro and in vivo effects of concentrated growth factor on cells and tissues, J. Biomed. Mater. Res. A 108 (6) (2020) 1338–1350.
[21] J. Chen, H. Jiang, A comprehensive review of concentrated growth factors and their novel applications in facial reconstructive and regenerative medicine, Aesth. Plast. Surg. 44 (3) (2020) 1047–1057.
[22] G. Li, H. Wang, Novel applications of concentrated growth factors in facial rejuvenation and plastic surgery, Facial Plast. Surg. 40 (1) (2023) 112–119.
[23] H. Li, X. Zhang, K.A. Ameer, X. Zhang, W. Du, S. Mei, X. Li, Clinical observation of concentrated growth factor (CGF) combined with iliac cancellous bone and composite bone material graft on postoperative osteogenesis and inflammation in the repair of extensive mandibular defects, Journal of stomatology, oral and maxillofacial surgery. 124 (6) (2023) 101472.
[24] Y. Zhang, T. Wang, D. Zhang, J. Li, X. Yue, W. Kong, X. Gu, Z. Jiao, C. Yang, Thermosensitive hydrogel loaded with concentrated growth factors promote bone repair in segmental bone defects, Front. Bioeng. Biotechnol. 10 (2022) 1039117.
[25] M. Ma, W. Shen, B. Li, M. Sun, D. Lin, L. Meng, Optimization of a concentrated growth factor/mesoporous bioactive glass composite scaffold and its application in rabbit mandible defect regeneration, Biomater. Sci. 11 (18) (2023) 6357–6372.
[26] L. Zhang, Z. Yuan, M. Shafiq, Y. Cai, Z. Wang, P. Nie, X. Mo, Y. Xu, An injectable integration of autologous bioactive concentrated growth factor and gelatin methacrylate hydrogel with efficient growth factor release and 3D spatial structure for accelerated wound healing, Macromol. Biosci. 23 (4) (2023) e2200500.
[27] S. Lian, Z. Mu, Z. Yuan, M. Shafiq, X. Mo, W. Mu, Methacrylated gelatin and platelet-rich plasma based hydrogels promote regeneration of critical-sized bone defects, Regen Biomater 11 (2024) rbae022.
[28] T. Kaibara, E. Kondo, M. Matsuoka, K. Iwasaki, T. Onodera, K. Sakamoto, Y. Oda, Z. I. Tanei, D. Momma, S. Tanaka, N. Iwasaki, Atelocollagen-associated autologous chondrocyte implantation for the repair of large cartilage defects of the knee: results at three to seven years, J. Orthop. Sci. 29 (1) (2023) 207–216.
[29] C. Chen, D. Wu, Z. Wang, L. Liu, J. He, J. Li, B. Chu, S. Wang, B. Yu, W. Liu, Peptide-based hydrogel scaffold facilitates articular cartilage damage repair, ACS Appl. Mater. Interfaces 16 (9) (2024) 11336–11348.
[30] W. Wei, Y. Ma, X. Yao, W. Zhou, X. Wang, C. Li, J. Lin, Q. He, S. Leptihn, H. Ouyang, Advanced hydrogels for the repair of cartilage defects and regeneration, Bioactive materials. 6 (4) (2021) 998–1011.
[31] Y. Cao, H. Zhang, M. Qiu, Y. Zheng, X. Shi, J. Yang, Biomimetic injectable and bilayered hydrogel scaffold based on collagen and chondroitin sulfate for the repair of osteochondral defects, Int. J. Biol. Macromol. 257 (Pt 1) (2023) 128593.
[32] Y. Shiromoto, Y. Niki, T. Kikuchi, Y. Yoshihara, T. Oguma, K. Nemoto, K. Chiba, A. Kanaji, M. Matsumoto, M. Nakamura, Increased migratory activity and cartilage regeneration by superficial-zone chondrocytes in enzymatically treated cartilage explants, BMC Musculoskelet. Disord. 23 (1) (2022) 256.
[33] Q. Li, H. Yu, F. Zhao, C. Cao, T. Wu, Y. Fan, Y. Ao, X. Hu, 3D printing of microenvironment-specific bioinspired and exosome-reinforced hydrogel scaffolds for efficient cartilage and subchondral bone regeneration, Adv Sci (Weinh) 10 (26) (2023) e2303650.
[34] P. Gonzalez-Fernandez, C. Rodríguez-Nogales, O. Jordan, E. Allémann, Combination of mesenchymal stem cells and bioactive molecules in hydrogels for osteoarthritis treatment, Eur. J. Pharm. Biopharm. 172 (2022) 41–52.
[35] Z. Wei, H. Ye, Y. Li, X. Li, Y. Liu, Y. Chen, J. Yu, J. Wang, X. Ye, Mechanically tough, adhesive, self-healing hydrogel promotes annulus fibrosus repair via autologous cell recruitment and microenvironment regulation, Acta Biomater. 178 (2024) 50–67.
[36] B.N. Singh, A. Nallakumarasamy, S. Sinha, A. Rastogi, S.P. Mallick, S. Divakar, P. Srivastava, Generation of hybrid tissue engineered construct through embedding autologous chondrocyte loaded platelet rich plasma/alginate based hydrogel in porous scaffold for cartilage regeneration, Int. J. Biol. Macromol. 203 (2022) 389–405.
[37] S. Ichiyama-Kobayashi, K. Hata, K. Wakamori, Y. Takahata, T. Murakami, H. Yamanaka, H. Takano, R. Yao, N. Uzawa, R. Nishimura, Chromatin profiling identifies chondrocyte-specific Sox9 enhancers important for skeletal development, JCI Insight 9 (11) (2024).
[38] M. Wu, S. Wu, W. Chen, Y.P. Li, The roles and regulatory mechanisms of TGF-β and BMP signaling in bone and cartilage development, homeostasis and disease, Cell Res. 34 (2) (2024) 101–123.
[39] R.D. Chavez, G. Coricor, J. Perez, H.S. Seo, R. Serra, SOX9 protein is stabilized by TGF-β and regulates PAPSS2 mRNA expression in chondrocytes, Osteoarthr. Cartil. 25 (2) (2017) 332–340.
[40] Y. Wei, L. Luo, T. Gui, F. Yu, L. Yan, L. Yao, L. Zhong, W. Yu, B. Han, J.M. Patel, J. F. Liu, F. Beier, L.S. Levin, C. Nelson, Z. Shao, L. Han, R.L. Mauck, A. Tsourkas, J. Ahn, Z. Cheng, L. Qin, Targeting cartilage EGFR pathway for osteoarthritis treatment, Sci. Transl. Med. 13 (576) (2021).
[41] A.H.F. Alnasraui, I.H. Joe, S. Al-Musawi, Design and synthesize of folate decorated Fe3O4@au-DEX-CP nano formulation for targeted drug delivery in colorectal cancer therapy: in vitro and in vivo studies, Journal of Drug Delivery Science and Technology. 87 (2023) 104798.
[42] F.S. Abdulwahid, A.J. Haider, S. Al-Musawi, Effect of laser parameter on Fe3O4 NPs formation by pulsed laser ablation in liquid, AIP Conf. Proc. 2769 (1) (2023) 020039.
[43] A. Haider, M. Al-Kinani, S. Al-Musawi, Preparation and characterization of gold coated super paramagnetic Iron nanoparticle using pulsed laser ablation in liquid method, Key Eng. Mater. 886 (2021) 77–85.